

A Spatiotemporal Framework for Information Freshness in IoT Uplink Networks

Mustafa Emara^{*†}, Hesham ElSawy[‡], Gerhard Bauch[†]

^{*} Next Generation and Standards, Intel Deutschland GmbH, Neubiberg, Germany

[†] Institute of Communications, Hamburg University of Technology, Hamburg, Germany

[‡] Electrical Engineering Department, King Fahd University of Petroleum and Minerals, Dhahran, Saudi Arabia

Email: {mustafa.emara@intel.com, hesham.elsawy@kfupm.edu.sa, bauch@tuhh.de}

Abstract—Timely message delivery is a key enabler for Internet of Things (IoT) and cyber-physical systems to support wide range of context-dependent applications. Conventional time-related metrics, such as delay, fails to characterize the timeliness of the system update or to capture the freshness of information from application perspective. Age of information (AoI) is a time-evolving measure of information freshness that has received considerable attention during the past years. In the foreseen large-scale and dense IoT networks, joint temporal (i.e., queue aware) and spatial (i.e., mutual interference aware) characterization of the AoI is required. In this work we provide a spatiotemporal framework that captures the peak AoI for large scale IoT uplink network. To this end, the paper quantifies the peak AoI for large-scale cellular network with Bernoulli uplink traffic. Simulation results are conducted to validate the proposed model and show the effect of traffic load and decoding threshold. Insights are driven to characterize the network stability frontiers and the location-dependent performance within the network.

Index Terms—Age of information, spatiotemporal models, Internet of Things, queueing theory, stochastic geometry

I. INTRODUCTION

The timeliness and retainability of continuous updates of nodes within a system are overarching requirements among different technology segments, such as vehicular, industrial Internet of Things (IoT) and cellular [1], [2]. This implies continuous information update about the real-time state between a given VRU and its targeted cluster of vehicles [3]. The proposed age of information (AoI) metric in [4] characterizes the freshness of information at the receiver and has received increasing attention in the past years. The age at a given time stamp (i.e., observation point) is defined as the current time stamp minus the time at which the observed state (or packet) was generated [5]. Compared to traditional time metrics (e.g. delay and jitter), AoI assists in achieving timely updates in a way those traditional metrics do not [6], [7].

The traffic generated by the existing IoT devices highly impact the AoI and the overall network performance. IoT traffic can be categorized into time and event triggered [8]. Time-triggered events generate periodic traffic as in vehicular communications, smart grids and wireless sensor networks [9]. In such segments, a central entity collects status updates from multiple nodes (e.g., sensors, vehicles and monitors) through wireless channels. A critical challenge is how to maintain timely status updates over all the connected nodes [10]. To this end, characterizing the AoI leads to informed designs to

enhance the performance of time-critical applications. Moreover, event triggered traffic are dependent on external events or critical information reporting. In this paper, we consider Bernoulli-based traffic model that mimic the aforementioned scenarios to analyze the peak AoI in uplink IoT networks.

Based on the foreseeable large number of deployed devices [11], interference might hinder timely updates of a given link of interest. In order to characterize the network-wide mutual interference, stochastic geometry is a prominent framework that can be leveraged [12]–[14]. However, considerations of the temporal evolution was not considered, as the full-buffer assumption at the transmitter side is widely adopted. To account for the temporal domain, recent efforts have integrated queueing theory with stochastic geometry, which offers a full spatiotemporal characterization for large-scale networks [15]–[19]. Following such a spatiotemporal analysis of the network, AoI was studied under a stochastic geometry framework in [20], where lower and upper bounds for the average AoI were derived. Moreover, AoI under a spatiotemporal framework has recently been investigated in [19], where the authors investigated different scheduling techniques to optimize the peak AoI under a spatiotemporal framework. To this end, large scale spatiotemporal IoT analytical framework for peak AoI characterization under different traffic loads is still an open research problem.

Throughout this work, we provide an analytical framework to characterize peak AoI that entails macroscopic and microscopic scales of uplink large scale IoT networks. Peak AoI is considered throughout this work due to its peak-characterization of the AoI compared to the average AoI, which fails to capture the underlying variance [19], [22]. For the macroscopic aspect, tools from stochastic geometry are adopted to account for the mutual interference among active devices (i.e., position dependent). Tools from queueing theory are employed to characterize the microscopic queue evolution at each device. To track the queue status at a given time stamp, a discrete time Markov chain (DTMC) is employed for each device. Expressions for the distribution of the coverage probability (i.e., meta distribution) are derived, which entails the effect of the traffic arrival. In addition, temporal distribution and the peak AoI are presented. To the best knowledge of the authors, this paper presents the first spatiotemporal framework that characterizes peak AoI within an uplink IoT network.

Throughout this paper, we adopt the following notation. Matrices and vectors are represented as upper-case and lower-case boldface letters (\mathbf{A} , \mathbf{a}), respectively. The indicator function is denoted as $\mathbb{1}_{\{a\}}$ which equals 1 if the expression a is true and 0 otherwise. In addition, $\mathbf{1}_m$ and \mathcal{I}_m denote, respectively, an all ones vector and matrix of dimension $m \times m$. In addition, identity matrix of dimension m is represented via \mathbf{I}_m . The complement operator is denoted by the over-bar (i.e., $\bar{v} = 1 - v$). The notations $\mathbb{P}\{\cdot\}$ and $\mathbb{E}\{\cdot\}$ denote the probability of an event and its expectation.

The rest of the paper is organized as follows. Section II provides the system model, the underlying physical and medium access control (MAC) assumptions, and the peak AoI characterization. Section III shows the macroscopic inter-device queueing interactions in terms of mutual interference. The proposed queueing model along with the microscopic intra-device interactions among the queues are presented in Section IV. Simulation results are presented in Section V and Section VI summarizes the work.

II. SYSTEM MODEL

A. PHY layer parameters

Throughout this paper, the base stations (BSs) are spatially distributed according to Φ with spatial intensity λ BS/km². The IoT devices point process Ψ is constructed such that within the Voronoi cell of every BS $b_i \in \Phi$, a device is dropped uniformly and independently. Single antennas are employed at all devices and BSs. An unbounded path-loss propagation model is adopted such that the signal power attenuates at the rate $r^{-\eta}$, where r is the distance and $\eta > 2$ is the path-loss exponent. Small-scale fading is assumed to be multi-path Rayleigh fading, where the intended and interference channel power gains h and g , respectively, are exponentially distributed with unity power gain. All channel gains are assumed to be spatially and temporally independent and identical distributed (i.i.d.). Fractional path-loss inversion power control is considered at the devices with compensation factor ϵ . Accordingly, the transmit power of an UE located r meters away from its serving BS is given by $\rho r^{\eta\epsilon}$, where ρ is a power control parameter to adjust the average received power at the BS [21].

B. MAC layer parameters

The proposed framework considers a synchronized and time slotted system, in which a new packet is generated at a generic device based on an i.i.d. Bernoulli traffic generation model, with per-slot inter-packet arrival probability of $\alpha \in (0, 1]$. A first-come first-serve queue is considered at each device, where failed packets are persistently retransmitted till successful reception. A packet is successfully decoded at its serving BS if the received signal to interference ratio (SIR) is larger than a predefined threshold θ . In case of successful decoding, that serving BS transmits an ACK through an error-free channel so the device can remove this intended packet from its respective queue. In case of failed decoding, the serving BS sends out a NACK and the packet remains at the head of the device's queue, awaiting a new transmission attempt in the next time slot. In Fig. 1, a snapshot realization of the network

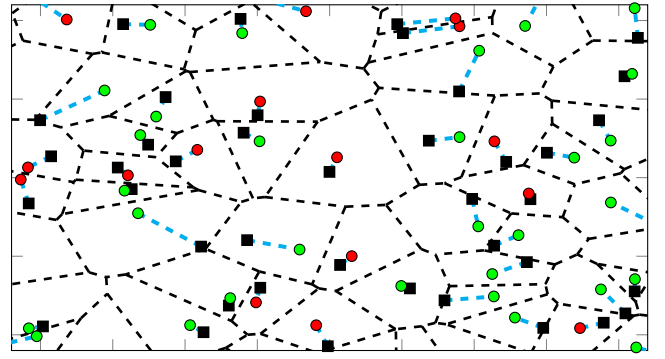


Fig. 1: A network realization for $\theta = 1$ and $\alpha = 0.25$ packets/slot. Black squares depict the BSs while green and red circles represent idle and active IoT devices, respectively. The Voronoi cells of the BSs are denoted by the dashed black lines while the dashed cyan lines denote the associations of the devices to their serving BSs.

is shown. At a given time slot two different panoramas of devices can be observed; i) non-active devices (i.e., devices with empty queues) ii) devices with packets in their queues due to either a packet arrival event or failed transmission attempts of backlogged packets¹.

C. Age of Information

As mentioned in Section I, AoI quantifies the freshness (i.e., timeliness) of information transmitted by the devices within the network [4]. For the considered time slotted system and a typical link, the AoI $\Delta_o(t)$, tracks the AoI evolution with time as shown in Fig. 2. Assume that the i th packet is generated at time $Y_o(t)$, then $\Delta_o(t+1)$ is computed recursively as

$$\Delta_o(t+1) = \begin{cases} \Delta_o(t) + 1, & \text{transmission failure,} \\ t - Y_o(t) + 1, & \text{otherwise} \end{cases} \quad (1)$$

Through this paper, we consider the peak AoI which is defined as the value of age achieved immediately before receiving the i -th update [22]. To this end, conditioned on a fixed, yet generic spatial realization, the peak AoI, as observed from Fig. 2, is computed as

$$\mathbb{E}\{\Delta^p|\Phi\} = \mathbb{E}^!\{\mathcal{I}_o + \mathcal{W}_o|\Phi\}, \quad (2)$$

where $\mathbb{E}^!\{\cdot\}$ is the reduced Palm expectation [14], \mathcal{I}_o and \mathcal{W}_o denote the inter-arrival time between consecutive packets and the waiting of a generic packet time in the queue, respectively. In order to characterize the peak AoI, one must compute the waiting time of a generic packet within the queue, which depends on, among other parameters, the traffic model, queue distribution and network-wide aggregate interference. In the remaining of this paper, we will provide a spatiotemporal framework that characterizes the peak AoI.

¹To analyze the location-dependent performance of the network, we consider a static network where for a generic network realization, Φ remains static over sufficiently large number of time slots, while channel fading, queue states, and device activities change from one time slot to another.

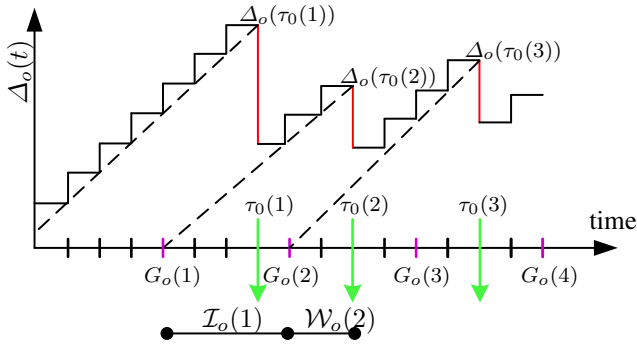


Fig. 2: AoI evolution of a typical link. The time stamps $G_o(n)$ and $\tau_o(n)$ denote the time at which the n -th packet was generated and successfully delivered. $\mathcal{I}_o(1)$ and $\mathcal{W}_o(2)$ denote the inter-arrival time and the waiting times.

III. MACROSCOPIC LARGE SCALE ANALYSIS

Through this section, the network-wide aggregate interference will be characterized. Focusing on a fixed arbitrary spatial realization of Φ and Ψ , let $u_o \in \Phi$ and $b_o = \operatorname{argmin}_{b_o \in \Psi} \|u_o - b_o\|$ be a randomly selected UE and its serving BS, respectively. The transmission success probability is defined as

$$\begin{aligned}
 P_s(\theta) &= \mathbb{P}^{\dagger} \left\{ \frac{P_o h_o \|u_o - b_o\|^{-\eta}}{\sum_{u_i \in \Phi \setminus u_o} a_i P_i g_i \|u_i - b_o\|^{-\eta}} > \theta | \Phi, \Psi \right\}, \\
 &\stackrel{(a)}{=} \prod_{r_i \in \Phi_o} \mathbb{E}^{\dagger} \left[\left(\frac{1}{1 + \frac{a_i \theta P_i r_o^{\eta(1-\epsilon)}}{\rho r_i^{\eta}}} \right) | \Phi, \Psi \right], \\
 &\stackrel{(b)}{=} \prod_{r_i \in \Phi_o} \left(\frac{\bar{\chi}}{1 + \frac{\theta P_i r_o^{\eta(1-\epsilon)}}{\rho r_i^{\eta}}} + \chi \right)
 \end{aligned} \quad (3)$$

where $\mathbb{P}^{\dagger}\{\cdot\}$ is the reduced Palm probability, P_o is the uplink transmit power of the typical device, $r_o = \|u_o - b_o\|$, $\Phi_o = \{\|b_o - \{ \Phi \setminus u_o \}\|\}$ represents the set containing distances between the interfering devices and BS of interest. In addition, a_i and P_i denote the i -th interference device activity profile and its uplink transmit power, respectively. The step (a) follows from the exponential distribution of the channel gains (i.e., h_o and h_i). Furthermore, the step b follows as $a_i \sim \text{Bernoulli}(\alpha)$. Finally, $\bar{\chi}$ is the spatially averaged idle probability, which is dependent on the queue distribution.

Spatially, the transmission success probabilities are random variables that are location dependent. The meta distribution characterizes the transmission success probabilities variation across the network [23], [24] as

$$\bar{F}(\theta, \delta) = \mathbb{P}^{\dagger}\{P_s(\theta) > \delta | \Phi, \Psi\}, \quad (4)$$

where δ is the percentile of devices within the network that can achieve $P_s(\theta)$. For uplink transmission with fractional power control, the conditional distribution of the transmission success

probabilities, where the beta approximation was utilized [25], [23] to approximate the meta distribution $f_{P_s}(\omega)$ as

$$F(\theta, \alpha) \approx I_{\alpha} \left(\frac{M_1 (M_1 - M_2)}{(M_2 - M_1^2)}, \frac{(1 - M_1) (M_1 - M_2)}{(M_2 - M_1^2)} \right), \quad (5)$$

where $I_{\alpha}(a, b) = \int_0^{\alpha} t^{a-1} (1-t)^{b-1} dt$ is the regularized incomplete beta function, M_1 and M_2 are the first and second moments of P_s . The approximations of P_s moments are given by the following lemma.

Lemma 1. *The moments of the transmission success probabilities in an uplink network with steady state queue idle probability χ , SIR threshold θ , path-loss exponent η , and fractional path-loss inversion compensation factor ϵ , are approximated by \bar{M}_b given in eq.(6), where χ is the residual interference intensity seen by the link and $\gamma(a, y) = \int_0^b t^{a-1} e^{-t} dt$ is the lower incomplete gamma function.*

Proof. See Appendix A ■

It is observed from Lemma 1 that the macroscopic network-wide aggregate characterization of the network depends on the queues evolution, via χ . In order to capture such interdependency, we first resort to the discretization of the meta distribution. Categorizing the devices within the network into classes is not feasible due to the continuous support of $P_s(\theta) \in (0, 1)$, which will lead to infinite number of classes. For practicality, the distribution in (5) is quantized into N quality of service (QoS) classes based on the importance criteria [18]. The network categorization process of the distribution in (5) for the n -th class is based first on computing ω_n as

$$F_{P_s}(\omega_n) - F_{P_s}(\omega_{n+1}) = \int_{\omega_n}^{\omega_{n+1}} f_{P_s}(\omega) d\omega = \frac{1}{N}, \quad (7)$$

where $n \in [1, 2, \dots, N]$. Afterwards, the discrete probability mass function d_n (i.e., $\mathbb{P}\{P_s = d_n\} = \frac{1}{N}$) can be evaluated using Bisection method as

$$\int_{\omega_n}^{d_n} f_{P_s}(\omega) d\omega = \int_{d_n}^{\omega_{n+1}} f_{P_s}(\omega) d\omega. \quad (8)$$

The computation of d_n , $\forall n = [1, 2, \dots, N]$ via eq. (7) and (8) quantizes the meta distribution into N equiprobable classes as shown in Fig. 3. The queue's service rate of a device belonging to the n -class is determined by d_n . Finally, in order to fully evaluate d_n , one needs first to compute χ which is dependent on the queue characteristics as presented in the next section.

IV. MICROSCOPIC QUEUEING THEORY ANALYSIS

The mathematical model for the microscopic scale (i.e., queue evolution) at the devices will be presented in this section. In the proposed framework, the device's location-dependency is captured via its departure probability (i.e. QoS class dependent), which is static over a sufficiently large number of time slots. However, the departure probability for each queue is still random and independent from one time slot to another due to the independent random variations of the channel gains and activity profiles of the interfering devices. Consequently, a Geo/Geo/1 queueing model is adopted to track

$$\tilde{M}_b = \int_0^\infty \exp \left\{ -z - \frac{2z^{1-\epsilon}}{\eta} \int_{\mathbb{1}\{\epsilon=1\}}^\infty y^{\frac{2}{\eta}-1} \left(1 - \left(\frac{y+\theta\chi}{y+\theta}\right)^b\right) \gamma \left(1 + \epsilon, zy^{\frac{2}{\eta(1-\epsilon)}}\right) dy \right\} dz, \quad (6)$$

$$\stackrel{(\epsilon=1)}{=} \exp \left\{ -\frac{2}{\eta} \sum_{n=1}^b \binom{b}{n} \frac{(-1)^{n+1} (\bar{\chi}\theta)^n}{n - \frac{2}{\eta}} {}_2F_1 \left(n, n - \frac{2}{\eta}, n + 1 - \frac{2}{\eta}, -\theta \right) \right\}.$$

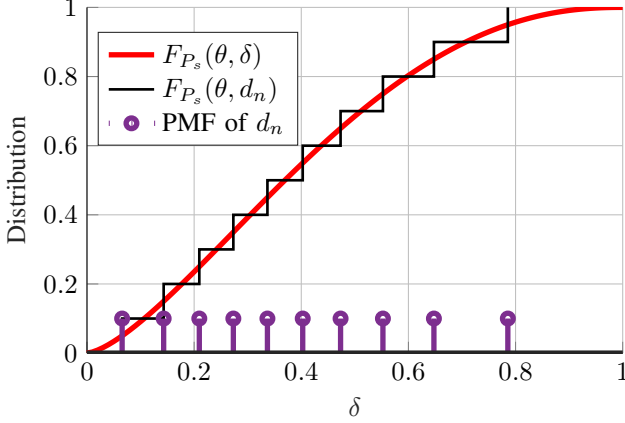


Fig. 3: Quantized meta distribution for $N = 10$, hypothetical $\chi = 0.5$, $\theta = 5$ dB, $\eta = 4$ and $\epsilon = 1$.

the queue evolution at each device, where Geo stands for geometric inter-arrival and departure processes. It is important to note that the geometric departure is an approximation that capitalizes on the negligible temporal correlation of the departure probabilities once the location-dependent QoS class is determined [18]. To this end, the queue transitions for a device within the n -th class are captured through the following probability transition matrix

$$\mathbf{P}_n = \begin{bmatrix} \bar{\alpha} & \alpha & & & \\ \bar{\alpha}d_n & \alpha d_n + \bar{\alpha}d_n & \alpha\bar{d}_n & & \\ & \bar{\alpha}d_n & \alpha d_n + \bar{\alpha}d_n & \alpha\bar{d}_n & \\ & & \ddots & \ddots & \ddots \end{bmatrix}. \quad (9)$$

To analyze the queue's stability, one is interested to determine the critical arrival rate after which the probability of having unstable queues starts to dominate and the queue's idle probability is zero [26]. Mathematically, for the DTMC in (9) to be stable, the equality $\frac{\alpha}{d_n} < 1$ must be satisfied. For unstable DTMCs, the idle probability is naturally 0. To this end, let $\mathbf{x}_n = [x_{0,n} \ x_{1,n} \ x_{2,n} \ \dots]$ be the steady state probability vector of the n -th class, where $x_{i,n}$ is the probability that a device belonging to the n -th class has i packets. The idle probability of device in the j -th class is evaluated as [27]

$$x_{i,n} = R_n^i \frac{x_{0,n}}{d_n}, \quad \text{where } R_n = \frac{\alpha\bar{d}_n}{\bar{\alpha}d_n}, \quad \text{and } x_{0,n} = \frac{d_n - \alpha}{d_n}. \quad (10)$$

Resorting to the mean field theory, the spatially averaged idle probability χ that is required to evaluate $F(\theta, \delta)$, is computed by averaging over the N classes temporal idle probabilities as

$$\chi = \frac{1}{N} \sum_{n=1}^N x_{0,n}. \quad (11)$$

Algorithm 1 Iterative computation of $F(\theta, \delta)$ and χ

```

Input ( $\alpha, \eta, \epsilon, \theta, N, \varphi$ )
initialize  $\chi$ 
while  $\|\chi^k - \chi^{k-1}\| \geq \varphi$  do
    Compute the moments  $\tilde{M}_b$  from Lemma 1
    Evaluate  $F(\theta, \alpha)$  based on (5)
    Compute  $d_i, \forall i = [1 \dots N]$  from the Discretized
     $F(\theta, \alpha)$  based on (7) and (8)
    for  $n = [1, 2, \dots, N]$  do
        if  $\alpha < d_n$  then
            Compute  $x_{0,n}$  based on (10)
        else
            Set  $x_{(0,n)} = 0$ 
        end if
    end for
    Compute  $\chi$  based on (11)
    Increment k
end while
Output:  $F(\theta, \delta)$  and  $\chi$ 
end Input

```

Once the queue distribution is characterized, one can proceed with evaluating the temporal distribution of a generic packet within the considered Geo/Geo/1 queue, which is the major component in computing the peak AoI as explained in Section II-C. As mentioned earlier, let \mathcal{W}_n be the waiting time in the queue for a packet at a device belonging to the n -th class and $\mathcal{W}_o^m = \mathbb{P}\{\mathcal{W}_o = m\}$. The waiting time for the n -th class is

$$\mathcal{W}_n^m = \begin{cases} \frac{d_n - \alpha}{d_n}, & m = 0 \\ \sum_{v=1}^i x_{v,n} \binom{i-1}{v-1} d_n^v (1-d_n)^{i-v} & m \geq 1. \end{cases} \quad (12)$$

Finally, by plugging eq.(12) in eq.(2), the network-wide peak AoI of a device within the n -th class is computed as

$$\mathbb{E}\{\Delta^p | \Phi\} = \frac{1}{\alpha} + \frac{1}{N} \left(\sum_{\varrho=1}^N \sum_{k=0}^{\infty} \mathcal{W}_{\varrho}^k k \right). \quad (13)$$

It is clear that to evaluate the peak AoI, the queue distribution is required, which in turn is dependent on the network-wide aggregate interference, via d_n . To solve such interdependency, Algorithm 1 is presented which converges uniquely to a solution by virtue of fixed point theorem [28].

V. SIMULATION RESULTS

In this section, the proposed spatiotemporal framework for the Bernoulli traffic is first validated. Afterwards, insights on the temporal distribution and peak AoI for different system

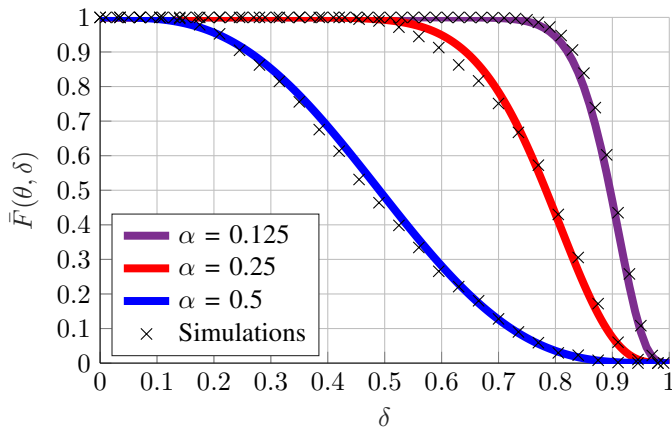


Fig. 4: Model verification for $\theta = 1$. Solid lines and black marks depict analysis and simulation, respectively.

parameters are demonstrated. First, framework validation is conducted via independent Monte Carlo simulations. The developed simulation framework incorporates microscopic averaging ensuring ergodicity, in which the steady state statistics of the queues employed at each device are collected. The simulation area is $10 \times 10 \text{ km}^2$ with a wrapped-around boundaries to ensure unbiased statistics imposed by the network boundary devices. In order to ensure that the queues are in a steady state, simulation is first initiated with all queues at the devices as being idle and then it runs for a sufficiently high number of time slots until the steady-state is reached. Let \hat{x}_0^t denotes the average idle steady state probability for the t -th iteration across all the devices within the network. Mathematically, the steady state is realized once $\|\hat{x}_0^k - \hat{x}_0^{k-1}\| < \varphi$, where φ is some predetermined tolerance. After steady state is reached, all temporal statistics are then gathered based on sufficiently large number of microscopic realizations. Unless otherwise stated, we consider the following parameters: $N = 10$, $\eta = 4$, $\rho = -90$, $\epsilon = 1$.

In Fig. 4 we show the meta distribution for $\theta = 1$ and different values of α . One can observe a close match between the simulation and the proposed framework, which implies that the iterative solution presented in Algorithm 1 in Section IV can capture the interdependency between the network-wide aggregate interference and the queues evolution. As the α increases, the capability of a given device to dispatch its packet generated at a given time slot deteriorates, due to the increased channel access and transmission attempts within the network. Accordingly, this packet will attempt retransmissions in consecutive time slots, thus, contributing to the aggregate interference on the devices that attempt transmissions in coming time slots. Such a consequential effect of increased traffic load affects the percentile of devices within the network to achieve a given transmission success probability, as illustrated via the meta distribution.

Moving to the AoI in Fig. 5, the peak AoI along with average waiting time are presented. As explained in Section II-C, the peak AoI depends on the inter-arrival and system waiting times of a randomly selected packet within the queue. First we investigate the effect of θ . As θ increases, packets are subjected to a more stringent requirement on their achieved

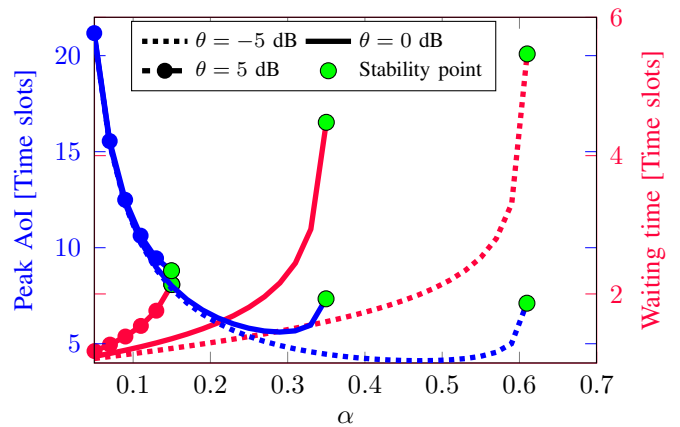


Fig. 5: Peak AoI (left) and average waiting time (right) for increasing packet generation periodicity (T) and θ .

SIR. This leads to increased retransmissions, thus, increasing the mutual interference due to lower idle probabilities. The increased mutual interference hinders the successful departure of the packets from their respective queues and lead to queue instability in some devices, yielding infinite waiting times and peak AoI. Moving to the arrival probability, for low values of α , the inter-arrival component dominates, yielding high values of peak AoI, while the waiting time is low. As α increases, the waiting times dominates, yielding an increase in the peak AoI till point of queue instability, as indicated by the stability point. The effect of θ on the stability frontiers can be explained in a similar fashion to that of Fig. 4, where increasing θ diminishes the stability region due to the increased network-wide aggregate interference.

Finally, Fig. 6 presents the peak AoI among the different QoS classes within the network. The shown classes are sorted in an ascending order with respect to d_n . For $\alpha = 0.05$, the inter-arrival times dominates the peak AoI, leading to a nearly-constant peak AoI over all the classes. The location-dependency is more clear for $\alpha = 0.15$ and $\alpha = 0.25$. Consequently, classes with lower indices experience large peak AoI due to their larger waiting times (i.e., effect of the location dependency captured via the meta distribution). For large traffic load (i.e., $\alpha = 0.25$), all except last two classes are unstable, which lead to infinite peak AoI.

VI. CONCLUSION

We present a tractable spatiotemporal mathematical framework to characterize the peak AoI in uplink IoT networks. We leverage tools from stochastic geometry to analyze the location-dependent performance of the network under Bernoulli traffic via the meta distribution. In addition, tools from queueing theory are utilized to track the queues evolution at each device and derive interference-aware expressions for the queue distribution and packets delay. To this end, an iterative algorithm is presented to solve the developed spatiotemporal model. Expressions for the packets waiting distribution within the queue and the peak AoI are provided. Simulation results are presented to validate the proposed spatiotemporal framework for different traffic load scenarios. The peak AoI along with the stability frontiers of the network are presented.

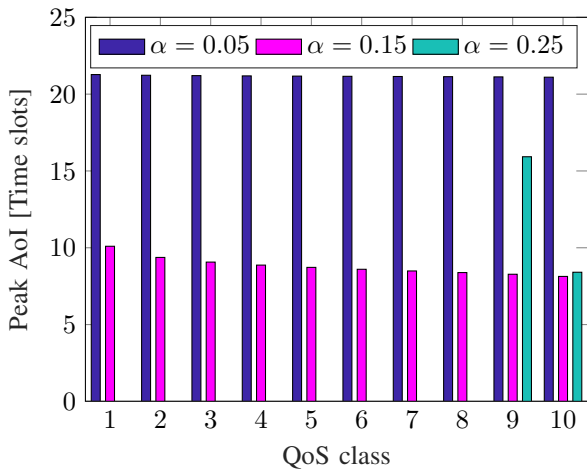


Fig. 6: Peak AoI for $N = 10$ QoS classes and $\theta = 5$ dB.

It is shown that the peak AoI highly depends on the spatial location, traffic arrival load, and decoding threshold.

REFERENCES

- [1] 3GPP, "TS 22.261 service requirements for next generation new services and markets," *3rd Generation Partnership Project (3GPP)*, v16.8.0, 2019,.
- [2] K. Kim and P. R. Kumar, "Cyberphysical systems: A perspective at the centennial," *Proceedings of the IEEE*, vol. 100, no. Special Centennial Issue, pp. 1287–1308, May 2012.
- [3] NGMNA, "Recommendations for NGMN KPIs and requirements for 5G," *Next Generation Mobile Networks Alliance*, 2016.
- [4] S. Kaul, R. Yates, and M. Gruteser, "Real-time status: How often should one update?" in *2012 Proceedings IEEE INFOCOM*, March 2012, pp. 2731–2735.
- [5] R. D. Yates and S. K. Kaul, "The age of information: Real-time status updating by multiple sources," *IEEE Transactions on Information Theory*, vol. 65, no. 3, pp. 1807–1827, March 2019.
- [6] M. A. Abd-Elmagid and H. S. Dhillon, "Average peak age-of-information minimization in UAV-assisted IoT networks," *IEEE Transactions on Vehicular Technology*, vol. 68, no. 2, Feb 2019.
- [7] E. T. Ceran, D. Gndz, and A. Gyrgy, "Average age of information with hybrid ARQ under a resource constraint," in *2018 IEEE Wireless Communications and Networking Conference (WCNC)*, April 2018.
- [8] F. Metzger *et al.*, "Modeling of aggregated IoT traffic and its application to an IoT cloud," *Proceedings of the IEEE*, vol. 107, no. 4, pp. 679–694, April 2019.
- [9] M. R. Palattella *et al.*, "Internet of things in the 5G era: Enablers, architecture, and business models," *IEEE Journal on Selected Areas in Communications*, vol. 34, no. 3, pp. 510–527, March 2016.
- [10] Z. Jiang *et al.*, "Timely status update in wireless uplinks: Analytical solutions with asymptotic optimality," *IEEE Internet of Things Journal*, vol. 6, no. 2, pp. 3885–3898, April 2019.
- [11] W. Ayoub *et al.*, "Internet of mobile things: Overview of LoRaWAN, DASH7, and NB-IoT in LPWANs standards and supported mobility," *IEEE Communications Surveys Tutorials*, pp. 1–1, 2018.
- [12] J. G. Andrews, F. Baccelli, and R. K. Ganti, "A tractable approach to coverage and rate in cellular networks," *IEEE Transactions on Communications*, vol. 59, no. 11, pp. 3122–3134, November 2011.
- [13] H. ElSawy *et al.*, "Modeling and analysis of cellular networks using stochastic geometry: A tutorial," *IEEE Communications Surveys Tutorials*, vol. 19, no. 1, pp. 167–203, Firstquarter 2017.
- [14] M. Haenggi, *Stochastic Geometry for Wireless Networks*. New York, NY, USA: Cambridge University Press, 2012.
- [15] Y. Zhong, T. Q. S. Quek, and X. Ge, "Heterogeneous cellular networks with spatio-temporal traffic: Delay analysis and scheduling," *IEEE Journal on Selected Areas in Communications*, vol. 35, no. 6, pp. 1373–1386, June 2017.
- [16] M. Gharbieh *et al.*, "Spatiotemporal model for uplink IoT traffic: Scheduling and random access paradox," *IEEE Transactions on Wireless Communications*, vol. 17, no. 12, pp. 8357–8372, Dec 2018.
- [17] H. H. Yang and T. Q. S. Quek, "Spatiotemporal analysis for SINR coverage in small cell networks," *IEEE Transactions on Communications*, pp. 1–1, 2019.
- [18] G. Chisci *et al.*, "Uncoordinated massive wireless networks: Spatiotemporal models and multiaccess strategies," *IEEE/ACM Transactions on Networking*, 2019.
- [19] Y. H. Yang *et al.*, "Locally adaptive scheduling policy for optimizing information freshness in wireless networks," in *2019 IEEE Global Communications Conference (GLOBECOM)*, Dec 2019, pp. 1–6.
- [20] Y. Hu, Y. Zhong, and W. Zhang, "Age of information in poisson networks," in *2018 10th International Conference on Wireless Communications and Signal Processing (WCSP)*, Oct 2018, pp. 1–6.
- [21] H. ElSawy and E. Hossain, "On stochastic geometry modeling of cellular uplink transmission with truncated channel inversion power control," *IEEE Transactions on Wireless Communications*, vol. 13, no. 8, pp. 4454–4469, Aug 2014.
- [22] L. Huang and E. Modiano, "Optimizing age-of-information in a multi-class queueing system," in *2015 IEEE International Symposium on Information Theory (ISIT)*, June 2015, pp. 1681–1685.
- [23] M. Haenggi, "The meta distribution of the sir in poisson bipolar and cellular networks," *IEEE Transactions on Wireless Communications*, vol. 15, no. 4, pp. 2577–2589, April 2016.
- [24] Y. Wang, M. Haenggi, and Z. Tan, "The meta distribution of the sir for cellular networks with power control," *IEEE Transactions on Communications*, vol. 66, no. 4, pp. 1745–1757, April 2018.
- [25] H. ElSawy and M. Alouini, "On the meta distribution of coverage probability in uplink cellular networks," *IEEE Communications Letters*, vol. 21, no. 7, pp. 1625–1628, July 2017.
- [26] R. M. Loynes, "The stability of a queue with non-independent inter-arrival and service times," *Mathematical Proceedings of the Cambridge Philosophical Society*, vol. 58, no. 3, p. 497520, 1962.
- [27] A. S. Alfa, *Applied discrete-time queues, second edition*. Springer-New York USA, 01 2015.
- [28] Y. Zhou and W. Zhuang, "Performance analysis of cooperative communication in decentralized wireless networks with unsaturated traffic," *IEEE Transactions on Wireless Communications*, vol. 15, no. 5, pp. 3518–3530, May 2016.
- [29] S. Singh, X. Zhang, and J. G. Andrews, "Joint rate and sinr coverage analysis for decoupled uplink-downlink biased cell associations in het-nets," *IEEE Transactions on Wireless Communications*, vol. 14, no. 10, pp. 5360–5373, Oct 2015.

APPENDIX A

PROOF OF LEMMA 1

The b -th moment of the transmission success probability can be derived from eq.(3) as

$$M_b = \mathbb{E}_{r_i, P_i, r_o} \left[\prod_{r_i \in \Phi_o} \left(\frac{\bar{\chi}}{1 + \frac{\theta P_i r_o^{\eta(1-\epsilon)}}{\rho r_i^\eta}} + 1 - \bar{\chi} \right)^b \right]. \quad (14)$$

Moreover, the uplink transmission power P_i of the i -th device is a random variable due to the employed fractional path-loss power control. This imposes correlation between the transmission powers of different devices due to the Voronoi sizes correlation of their serving BSs. Similar to [25], [29], the transmission power correlations are ignored for mathematical tractability. The interfering devices are approximated with the interference seen from an inhomogeneous Poisson point processes (PPP) $\tilde{\Phi} \in \mathbb{R}^2$ with the following intensity function $\lambda(x) = \lambda(1 - e^{-\pi\lambda\|x\|^2})$. Following [25, Theorem 1] via applying the mapping and displacement theorem on $\tilde{\Phi}$, the approximated expressions for the moments are derived, where the activity profile depicts the aggregate probability of having a packet within the queue awaiting transmission, which is $1 - \chi$, where χ is the aggregate idle probability.